IR-Active Matrix-Isolated Molecules (CO and CO_2) to Probe Host Crystal (N_2) Quality†

Martin Vetter, Matthias Jordan, Alexander P. Brodyanski, and Hans J. Jodl*

Fachbereich Physik, Universität Kaiserslautern, Erwin Schrödinger Strasse, 67663 Kaiserslautern, Germany

Received: October 29, 1999; In Final Form: February 16, 2000

The matrix isolation technique is a powerful technique for specific questions. But due to relatively high impurity concentrations (10^{-2}−10^{-4}) the impurity is not in a *real* matrix-isolated case, as in theoretical descriptions. In addition, due to sample preparation (cold deposition) the matrix resembles more an amorphous thin film rather than a *good* crystal, in terms of solid state physics. As a consequence, many spectroscopic data or phenomena were misinterpreted in the past. Therefore, we studied the *real* matrix-isolated case ($\sim 10^{-7}$) in pretty good bulk matrix material. Looking at impurity spectra (CO, CO_2, and their isotopes) and analyzing bandwidths, frequencies, and intensities as a function of temperature, we could characterize the quality of structural phase transitions of matrix and its hysteresis; we could unambiguously assign crystal field splitting to orientations of matrix-isolated particles in the host crystal; we could separate homogeneous from inhomogeneous bandwidth and discuss crystal quality of matrix; due to carefully determined integrated absorption intensities and known absorption coefficients, we were able to determine the real concentration of impurities in the matrix etc. Because of the improved FTIR technic (high sensitivity, resolution, accuracy) we studied in addition the overtone region of molecular excitations and investigated the kinetics of phase transitions; finally, we found spectroscopic evidence of impurity clusters and bands. Consequently, we are able to determine solubility limits of impurities in matrix (in our specific case this limit is about ppm).

1. Introduction

The matrix isolation technique was developed about 50 years ago in order to investigate the high chemical active or transient species. To reach this aim the species under study had to be fixed in their unstable or low stable states in inert matrices in relatively small concentrations. Therefore, some cryocrystals such as rare gas solids or solid N_2 and H_2 have been traditionally used as a matrix material and the samples have been prepared by some different low-temperature condensation methods at which the molecules or radicals of interest were trapped in host crystals.

At the beginning of the 1970s it was understood that the matrix isolation spectroscopy can render some important information on the physical aspects too. At first, it was related to (i) the influence of the matrix on the matrix-isolated (MI) molecule, (ii) the matrix changes around these species and the site effects, (iii) the interaction between the trapped molecules, and (iv) the dimer formation. In these "physical" investigations, the simple stable molecules (CO, CO_2, CH_4, OCS, NO, N_2O, etc.) have usually been used as MI species.

Considerable progress has been made toward a theoretical understanding of the vibrational and rotational shift for MI molecule in matrix. Under conditions of perfect isolation, these environmental frequency shifts are determined the solute−matrix interaction statistically averaged over translational and orientational motion of both interacting particles.[1−3] Some experimental information was also collected on the reaction of the matrixes to the insertion of these species into matrix (matrix sites effects) as well as on the influence of the different matrixes on the characteristics of the trapped molecules (matrix effects). The main efforts have been put to investigate these mutual effects at the insertion of linear molecules into rare gas solids. Three qualitatively different situations were observed:[4] a trapped molecule replaces one matrix atom only (single substitutional site), a MI particle occupies two nearest atom positions in a host crystal (double substitutional site), and an amorphous region of the matrix is formed around the impurity. Recently,[5] it was shown that only the first situation corresponds to the thermodynamic stable situation in the case of relatively small MI species—namely, so-called "single substitutional site".

Since in this technique the main emphasis was to study the characteristics of the defect or host crystal particles around it, less care was taken to consider correctly effects of the host crystal; therefore, site effects, polymer phenomena, temperature effects of the matrix, phase transitions of matrix, etc. were often misinterpreted as a behavior of the doped particle.

Our idea is to use the matrix isolation technique like an instrument to collect some important information on the host crystal. We believe that by monitoring the behavior of the impurity molecules carefully, we can probe the host crystal regarding such parameters, whose changes can affect the registered spectroscopic characteristics of the matrix-isolated molecules. The intermolecular distance, site symmetry, and orientational order belong to these parameters of the host crystal; i.e., by this approach we can gain information on the crystal quality, phase transition, possible orientational positions, orientational order parameter, local ordering around the impurity, etc. by investigating the spectroscopic characteristics of the matrix-isolated molecules. This idea is based on the following considerations.

The spectroscopic characteristics of a matrix-isolated molecule such as the vibrational frequency and the corresponding bandwidth depend on the interaction between the trapped molecule and the surrounding host particles (atoms or molecules), the thermal motion of both guest and host particles, and the host crystal perfection. Of course, the guest molecule

† Part of the special issue "Marilyn Jacox Festschrift".

10.1021/jp993845+ CCC: $19.00
Published on Web 04/01/2000

deforms the host crystal lattice around it. However, the displacement field around the impurity reflects the symmetry of the trapped molecule as well as the symmetry of the host crystal lattice and is quantitatively determined by the impurity−host crystal interaction too.[6,7] The relative displacement of the matrix particles in the vicinity of an impurity changes rapidly from the first shell of neighboring matrix particles to next ones. At distances more than $3R_0$ off an impurity, where R_0 is the radius of the first coordination sphere of the host cryocrystal, this displacement can be neglected with respect almost all impurity qualities. Furthermore, there is not any phase boundary between this deformed matrix area and perfect regions of the host crystal.[7] That is why we can presume that the matrix particles in an area deformed by an impurity−matrix interaction react to a variation of external conditions (pressure, temperature) qualitatively similar like the matrix particles in the perfect host crystal region. Because the number of the matrix-isolated molecules is very large (about 10^{13} at the admixture/matrix ratio of 10^{-7}) and these impurity molecules are randomly distributed in the host crystal, the experimental values for frequency and bandwidth of the matrix-isolated molecules are statistically averaged on the whole host crystal. Consequently, these values yield information on the long-range order in the host crystal. This means that the ensemble of matrix-isolated molecules senses the long-range order in the host crystal and, of course, senses the changes in the host crystal when the external parameters (pressure, temperature) are varied.

The main aim of this work is to prove our general idea. Using the matrix isolation technique we investigated the host crystal's crystal structure perfection, phase transitions, and possible orientational positions.

Solid nitrogen was selected as a host crystal consisting of IR-inactive molecules that possesses a phase transition ($T_{\alpha\rightarrow\beta}$ = 35.6 K) in the solid state. The low-temperature α-phase of this crystal is orientationally ordered and its structure corresponds to the *Pa*3 space group. The high-temperature β-phase of solid nitrogen has $P6_3/mmm$ crystal structure (so-called hcp structure) without any long-range orientational order ("plastic" phase). The IR-active linear molecules CO and CO_2 were chosen to probe indirectly this crystal at the admixture/matrix ratio of about 10^{-7}. Because the phase diagram of the N_2-CO_2 system is unknown up to now,[8] nothing is known about miscibility or solubility.

Our paper is structured as follows. The next section outlines our experimental procedure, such as sample preparation, determination of concentration, and spectroscopic details. The experimental results are presented together with the discussion in one section. We will focus on three different aspects: first, present a physical model of the behavior of linear guest molecules in *Pa*3 and hcp structures based on our spectroscopic data; second, interpret experimental values to probe host crystal qualities; third, discuss solubility limit and clustering of impurity molecules.

2. Experimental Section

We investigated nitrogen doped by CO and CO_2 molecules by FTIR studies in the temperature range from 10 to 90 K. The infrared spectra of samples were recorded in the spectral region of 2000−5000 cm^{-1} by a Fourier spectrometer (Bruker IFS 120 HR), equipped with a glowbar source, a KBr beam splitter, and a liquid nitrogen cooled InSb detector. The frequency resolution was varied from 0.007 to 0.037 cm^{-1} depending on the bandwidth of the investigated line. The optical cutoff filter for the spectral region 2000−3000 cm^{-1} was used to improve the signal-to-noise ratio. Besides the CO and CO_2 modes, the IR-active combined bands of the host crystals (such as sideband, two-vibron band) were also recorded. We used these combination bands as an internal standard to determine exactly the phase transition points in the host crystals.

A specially designed sample cell with diamond windows (accessible frequency range 10−43 000 cm^{-1}) was mounted on a closed-cycle cryostat coldfinger. The accuracy of the sample temperature stabilization coincided approximately with the accuracy of the temperature measurement during our experiments: a computer-controlled temperature variation. We measured the sample temperature with a standard Si diode with an accuracy of ±0.005 K in the temperature region 10−25 K and ±0.05 K at higher temperatures. The Si diode was directly attached to the sample cell. This Si diode was additionally calibrated by 9 standard points (melting points of H_2, Ne, O_2, N_2, CH_4; temperatures of the solid−solid phase transitions in CH_4, O_2, N_2) as well as by comparing the experimental temperature−pressure dependencies of the equilibrium vapor pressure for liquid Ne, O_2 and N_2 with the data.[9] This procedure allowed us to reach an absolute accuracy of the sample temperatures not less than ±0.02 K below 25 K and ±0.1 K below 100 K.

Matrix isolation (MI) technique used to work with an admixture/matrix (A:M) ratio of $\sim10^{-4}$; this high concentration can cause problems such as dimers, insolubility etc. In order to avoid any influence of the impurity interaction, we used an A:M ratio of $<10^{-6}$ to achieve the *real* MI case.

The samples must have high-quality structure to observe and to study the matrix-isolated molecules in the wide temperature region at such small concentrations. Furthermore, the initial sample structure had to correspond to the thermodynamic equilibrium crystal structure of the host crystal to investigate the equilibrium phase transitions and probe the host crystal qualities. The traditionally used deposition technique in MI produces too many defects in the matrix; therefore, we grew perfect crystal samples from the liquid.

The sample cell was evacuated ($\sim10^{-6}$ mbar), purged by the gas mixture at the room temperature, and repeatedly evacuated. The empty sample cell was cooled onto a temperature corresponding to the liquid phase of the matrix material. At a temperature a little higher than the melting point (1−2 K), the gas mixture was loaded into the cell at the pressure of 1.5 bar. After condensation at the same pressure, this liquid sample was slowly (3 K/h) cooled toward the melting point to grow slowly the crystal. Our crystal had the diameter of about 10 mm and thickness of about 1.2 mm. The grown crystals were completely transparent to visible light without any visible boundaries. As we will show below (Figures 3, 4), in our samples the fundamental bands of the CO and CO_2 molecules—matrix isolated in solid nitrogen—possess almost no residual inhomogeneous broadening caused by static crystal imperfections.

We applied different techniques to determine the impurity/matrix ratio: via partial pressure, via mass spectrometry, and via spectroscopy (absorption coefficient). The purity of used nitrogen gas was 99.999%. Two series experiments with different A:M were carried out. In the first series (A), we used this nitrogen gas with small traces of CO_2 molecules to probe the host crystal. The concentration of the CO_2 in our nitrogen gas was equal to 135 ppb, determined by mass-spectroscopic measurements. Only monomers of the CO_2 in N_2 crystal were observed in our middle IR spectra. The ν_3 fundamental mode of isotope $^{13}C^{16}O_2$ (concentration of isotopes in solid nitrogen was approximately 10^{-9}) was also clearly seen in IR absorption,

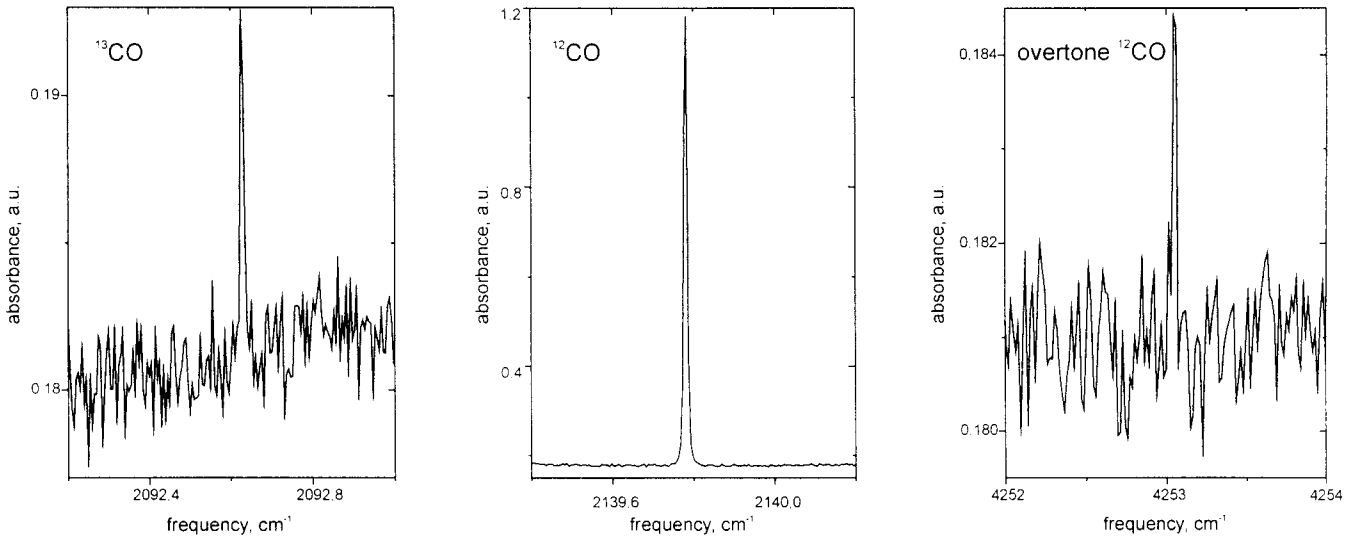

Figure 1. Internal vibrations of CO molecules matrix isolated in solid nitrogen. $T = 11$ K; $^{12}CO/N_2 \sim 5 \times 10^{-7}$; $^{13}CO/N_2 \sim 5 \times 10^{-9}$.

but only in the α-N_2 phase ($T < 35$ K). The integrated intensity ratio of the ν_3 vibrational bands of $^{13}C^{16}O_2$ and $^{12}C^{16}O_2$ was 0.0106 that coincides with the natural abundance (1.11%[10]).

In the second series (B) of experiments, we premixed 75 ppm of CO_2 gas with N_2 gas. Bands, which we assign to CO_2 clusters (see later), were observed in these samples as well as bands, which we assign to CO_2 molecules matrix isolated in solid nitrogen. It was very surprising to us that the integrated intensities of the ν_3 modes corresponding to the CO_2 molecules matrix isolated in solid N_2 were just the same for samples of series A and B. It could be suspected that small amount of CO_2 is permanently present either in our sample cell or in our sample preparation system. To exclude this hypothesis, we performed another experiment with pure oxygen in the same setup and found no traces of CO_2 molecules in our spectra. IR spectra of samples enriched with CO_2 (75 ppm in N_2) also contained lines that we assigned to CO molecules. Our CO_2 gas (purity 99.995%) contains the CO molecules as the residual contamination. Only monomer bands of the CO in N_2 crystal were observed in our spectra. IR absorption of isotope $^{13}C^{16}O$ fundamental mode as well as of the $^{12}C^{16}O$ overtone band was clearly observable at a temperature less than 25 K too. Figure 1 shows our experimental spectra of the CO molecules matrix isolated in solid N_2 at 10.9 K.

The ratio of the integrated intensities of the $^{13}C^{16}O$ and $^{12}C^{16}O$ fundamental bands was 0.0126 that is just the same as the natural abundance. The experimental integrated absorption I_{int} for the $0 \rightarrow 1$ and $0 \rightarrow 2$ transitions of the $^{12}C^{16}O$ in α-nitrogen at 10.9 K were $0.012\,61 \pm 0.000\,06$ cm^{-1} and $(9.9 \pm 2.7) \times 10^{-5}$ cm^{-1} respectively. Using the relation

$$c_{CO}(N_2) = V_{mol}(N_2)(I_{int}/\alpha_{CO})/L \qquad (1)$$

where $V_{mol}(N_2)$, α_{CO}, and L are a nitrogen molar volume,[11] the absolute absorption coefficients for the gaseous CO[12] and the thickness of our samples, respectively, we were able to estimate the concentration c of the CO molecules in the samples of the series B. It was shown by Legay-Sommaire and Legay[13] that the environmental effects may alter the absorption coefficients less than 20% which can be neglected in our consideration.

Consequently, we determined for both set of experiments the following impurity concentrations by optical spectroscopy and mass-spectroscopic investigations (Table 1).

TABLE 1: Concentration of the IR-Active Impurities in Our Sample

samples	$^{12}CO_2$	$^{13}CO_2$	^{12}CO	^{13}CO
A (N_2, 99.999%)	1.4×10^{-7}	$\sim 1.5 \times 10^{-9}$		
B (N_2 + 75 ppm CO_2	1.5×10^{-7}	$\sim 1.6 \times 10^{-9}$	5×10^{-7}	$\sim 5 \times 10^{-9}$

3. Results and Discussion

In this section we begin with the orientationally ordered α-phase. Next, we show how the matrix-isolated species react to the $\alpha-\beta$ phase transition. After that we will analyze the unusual feature of the matrix-isolated molecules behavior in the orientationally disordered β-nitrogen. It is very important to note that both series of our samples (A and B) were practically identical with respect to the spectroscopic results of the CO_2 molecules matrix isolated in solid nitrogen. At the end of this section we will discuss the CO_2 clusters in our samples with 75 ppm of CO_2.

3.1. IR Active Modes of CO and CO_2 Molecules in α-Nitrogen. In α- nitrogen the host molecules are oriented along the body diagonals of the cubic structure. In these orientational positions they accomplish librational motions only (~15°). The amplitude of this motion depends on the relation between the anisotropic part of the intermolecular interaction U_{anis} and the rotational constant B of the molecule. Using any simple combination rule for potential parameters of a mixture[14] and the known potential parameters of the CO, CO_2, and N_2 molecules (Lennard-Jones parameters, the quadrupole moments, etc.[8,11]), it is easy to show that the numerical values for U_{anis}/B for the CO and CO_2 molecules isolated in solid nitrogen are larger than this relation for the host crystal. This means that our guest molecules are oriented similarly to the host crystal molecules and the amplitude of their librational motion is at least as small as the one for the nitrogen molecules. Therefore, we can expect a qualitatively similar temperature behavior of the vibrational frequency and the bandwidth of these matrix-isolated molecules in comparison to the corresponding N_2 vibrons. On the other hand, the CO and N_2 molecules have almost the same size[15] whereas the CO_2 molecules are bigger than the host crystal molecules.[16] Consequently, the deformation of the matrix around the impurity must be substantially different for these two guest molecules. This circumstance must be reflected in the spectroscopic characteristics of the MI impurity too.

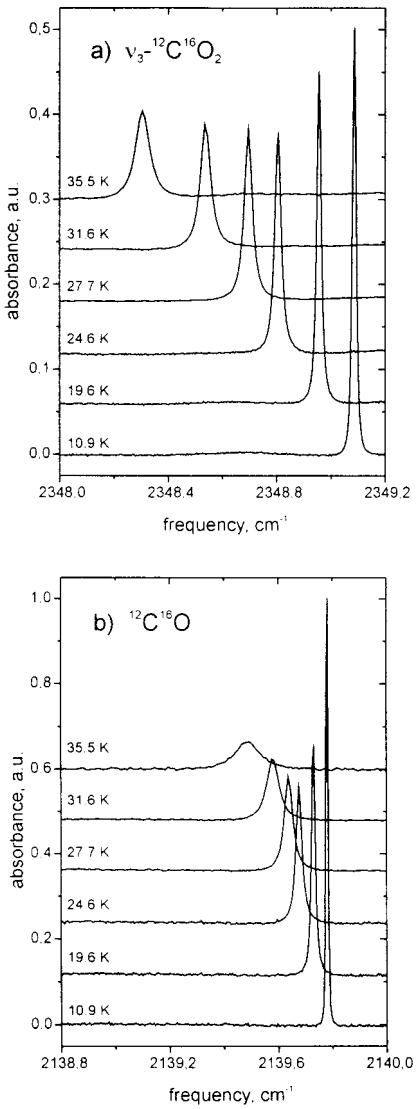

Figure 2. Temperature evolution of vibrational spectra of IR-active molecules matrix isolated in α-nitrogen. $CO_2/N_2 \sim 1.3 \times 10^{-7}$; $CO/N_2 \sim 5 \times 10^{-7}$.

The spectra of the $^{12}CO_2$ and ^{12}CO internal vibrations in α-nitrogen are shown in Figure 2. Two features are clearly visible: as the temperature increases, the band maxima of matrix-isolated species are shifted to lower energy and the bandwidths become larger. This behavior is qualitatively similar for *each* band of the MI species observed by us.

3.1.1. Bandwidth. Each of our matrix-isolated absorption bands had a symmetric profile (see Figure 2), and their shape can be described neither by a pure Lorentz nor by a pure Gauss function. Therefore, we opted for the Voigt function to describe the experimental band profiles, because this function corresponds to the convolution integral of the Lorentz and Gauss probability densities[17] and its characteristic function is traditionally used like the decay law of the vibrational amplitude at studies in the time domain. This choice allowed us to achieve very good agreement between the experimental and analytical profiles for all our spectra.

Figures 3 and 4 show the $^{12}CO_2$ and ^{12}CO bandwidth as a function of the temperature in α-phase of solid nitrogen, respectively. As can be seen, the CO band is essentially narrower than the CO_2 one at the low temperatures but possesses a substantially stronger dependency on the temperature.

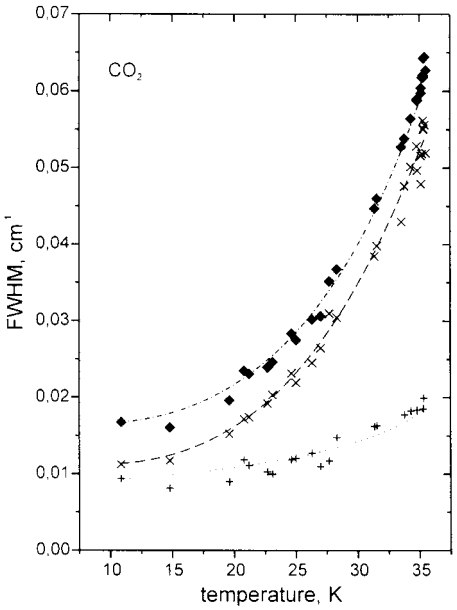

Figure 3. Bandwidth of the CO_2 vibration in α-nitrogen as a function of temperature: the spectral band shape at experimental values (diamond) was first deconvoluted into a Lorentzian (cross) and Gaussian (plus) band shape. On the basis of our model (see text), we fitted the Lorentzian data points (dashed line, calculation) and the Gaussian ones (dotted line, calculation) and modeled by that the experimental values (dash-dotted line, calculation).

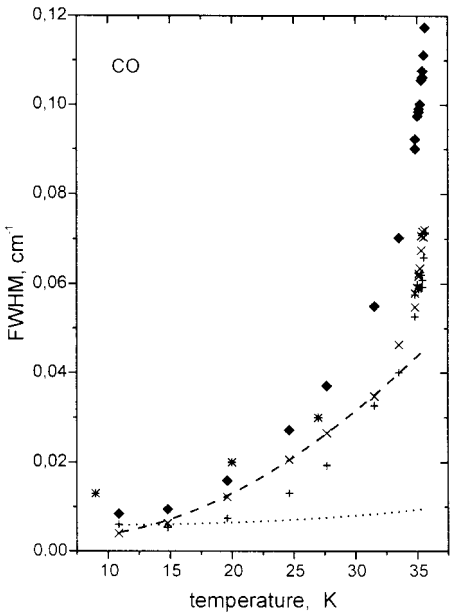

Figure 4. Bandwidth of the CO vibration in α-nitrogen as a function of temperature (star, experimental values[22]): the spectral band shape at experimental values (diamond) was first deconvoluted into a Lorentzian (cross) and Gaussian (plus) band shape. On the basis of our model (see text), we fitted the Lorentzian data points (dashed line, calculation) and the Gaussian ones (dotted line, calculation).

Although some experiments were dedicated to investigate the ν_3 mode of CO_2 trapped in solid nitrogen,[18−21] we were not able to find any information on the corresponding bandwidth. Dubost et al.[22] carefully investigated the CO matrix isolated in solid N_2 as a function of the CO-concentration at some temperature points. The fwhm values for the lowest concentration ($\sim 10^{-5}$ CO in N_2) investigated by them are shown in Figure 4 too. Their values are larger than ours and this discrepancy may be attributed to different sample preparation technique (the samples in ref 22 were obtained by spraying a gaseous mixture

of CO and N_2 onto a cold CsBr plate). Our fwhm values for the CO and CO_2 in α-nitrogen were comparable to the data for the vibron bands of pure nitrogen crystal at $T \leq 25$ K.[23,24]

Three groups of physical reasons are known to cause band broadening: inelastic (depopulation) processes, elastic (dephasing) processes, and a stochastic distribution of the local crystal fields originated by different kinds of crystal imperfections.[25] The first two processes are directly connected to the lifetime of the excited vibrational state and lead to a Lorentzian profile (so-called *homogeneous broadening*) whereas the latter broadening mechanism results in a Gaussian profile (so-called *inhomogeneous broadening*).

To separate the different broadening mechanisms occurring in our samples the Gaussian and Lorentzian contributions to the bandwidths were derived from their spectra. The temperature dependencies of these components as fit function are depicted in Figures 3 and 4 too. This deconvolution procedure is only a little bit questionable at 11 K, where the fwhm of the CO band and the apparatus resolution (0.007 cm^{-1}) almost coincided.

(a) Lorentzian Component of the Bandwidth. The temperature dependencies of the experimental Lorentzian fwhm for CO and CO_2 are very similar to each other (see Figure 3 and 4). This means that the relaxation mechanisms were the same for both excitations. At almost all temperatures (except near the $\alpha-\beta$ phase transition) the CO vibrations are characterized by a smaller Lorentzian bandwidth component than the $\nu_3(CO_2)$ excitations.

The exponential decay times corresponding to our Lorentzian fwhm for the CO and CO_2 in solid nitrogen were 840 and 450 ps at 14.8 K, respectively, and decreased to about 100 ps at 35 K. It is interesting to note that the low-temperature value of the $\nu_3(CO_2)$ decay time derived from our CO_2 Lorentzian bandwidth is very close to the $^{14}N_2$ vibron relaxation time in α-nitrogen and is substantially larger than the one for the stretching vibrations of the $^{15}N_2$ molecules dissolved in this $^{14}N_2$ crystal, measured by TR-CARS.[26] We think that this discrepancy may originate from the considerably higher concentration of the impurities (1.7% of $^{15}N_2$ in $^{14}N_2$ crystal). As was shown by Dubost et al.,[22] the impurity fwhm rises noticeably with increasing concentration of the same kind of impurities.

Let us analyze in more detail now the temperature dependencies of the Lorentzian bandwidth component for the systems investigated by us. The Lorentzian component of the impurity vibration bandwidth can be described as follows:

$$\Delta_L = T_1^{-1} + T_2^{*-1} \qquad (2)$$

where T_1 is the rate of population decay and T_2^* is the rate of pure dephasing.

The general expressions for T_1 and T_2 are given in ref 25 for the decay of phonon and vibron modes in pure crystals and in ref 27 for the specific case of impurity vibrations. Although the relaxation mechanisms are different in these two cases (pure and doped crystals), the final expressions for T_1^{-1} and for T_2^{*-1} are the same.

At low temperatures two basic assumptions may be made: (i) only cubic down-conversion processes contribute to the population decay of the impurity vibration; (ii) only the lowest order quartic processes contribute to the pure dephasing. These processes can be summarized as follows:

$$\text{depopulation processes} \quad \omega_{vib}^{imp} = \omega_{vib} + \omega_{ph} \qquad (3)$$

$$\text{dephasing processes} \quad \omega_{vib}^{imp} + \omega_{ph}^{m} - \omega_{ph}^{n} = \omega_{vib}^{imp} \qquad (4)$$

It is implied that the ω_{ph} is the frequency of a thermal bath phonon, including localized librational and translational motions of the impurity molecule, and the ω_{vib} in (3) is a frequency of any other internal molecular vibration in our system (host crystal vibrons, isotopes, etc.) whose values are lower than the frequency of the analyzed guest molecule.

TABLE 2: Parameters of the Relaxation Processes Determining Lorentzian Broadening of the CO and CO_2 Bandwidths in α-Nitrogen[a]

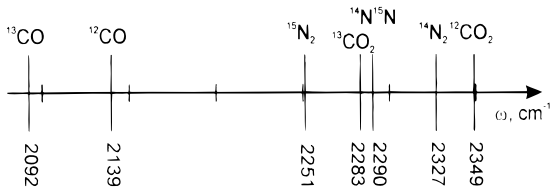

guest molecule	ω_{depop}	B_{depop}	ω_{deph}	B_{deph}
CO	47.2	0.003	31	0.08
CO_2	20.7	0.011	85.5	1.1

[a] All values are given in cm^{-1}.

Only one depopulation decay channel exists for the case of the ^{12}CO internal vibration in N_2 crystal at low temperatures; i.e., energy transfer to the isotope ^{13}CO. Owing to the extremely low concentration of impurities the contribution of this process to the main CO isotope Lorentzian bandwidth is expected to be very small.

Although many possibilities are in principle available like down processes for the $\nu_3(^{12}CO_2)$ vibrations, their inelastic relaxation is mostly governed by transferring energy to the host crystal vibrons, since the probability of the depopulation processes (3) is proportional to the occupation number $n_i = [\exp(\hbar\omega_i/kT) - 1]^{-1}$ of the phonon states with the frequency

$$\omega_i \equiv \omega_{depop} = \omega_{vib}^{imp} - \omega_{vib}$$

For the sake of simplicity, we choose only one average phonon frequency to model the dephasing processes; i.e., $\omega_{ph}^{m} = \omega_{ph}^{n} = \omega_{deph}$ in the eq 4. Then, the general formulas of[25,27] can be simplified:

$$\Delta_L = B_{depop}(1 + n_{depop}) + B_{deph}n_{deph}(1 + n_{deph}) \qquad (5)$$

Here B_{depop}, n_{depop} and B_{deph}, n_{deph} are the square of the effective anharmonic coupling coefficients and the occupation numbers of corresponding phonons (ω_{depop} and ω_{deph}) for the depopulation and dephasing processes, respectively. The values B_{depop}, B_{deph}, and ω_{deph} were obtained by fitting the experimental Lorentzian bandwidths with the formula (5). The parameters determined by this fitting procedure and the frequencies ω_{depop} involved are collected in Table 2. We interpret these results as follows.

The energy transfer from the excited $\nu_3(^{12}CO_2)$ state to the host crystal vibrons dominates at low temperatures. The pure dephasing of the CO_2 vibrations becomes nonnegligible at about 24 K and becomes the dominant process at temperatures higher than 30 K. The vibronic dephasing of the $^{12}CO_2$ molecules matrix isolated in solid nitrogen is governed by a localized mode with the frequency $\omega_{deph} = 85.5$ cm^{-1}, which results from the alteration of the distribution of normal modes of the N_2 crystal ($\omega_{Debye} \sim 58$ cm^{-1})[11] by inserting these guest molecules. It is hard to define exactly the origin of this localized mode (either translational or librational one) without direct calculations. However, according to our opinion, the assignment of this mode as the CO_2 librational mode is more plausible; as we already stated, the CO_2 libration is considerable different to the host

crystal librons, whereas the CO_2 translation is almost similar to the lattice translations.

The broadening of the CO internal vibrations by dephasing processes is nonnegligible at 11 K already and becomes the dominant process at temperatures higher than 20 K. The corresponding value of a suited mode in an elastic process ω_{deph} (31 cm^{-1}) is close to the frequency of the low-energy N_2 librational mode (32 cm^{-1}) as well as to the maximum of the density of phonon states of α-nitrogen.[11] This means that the CO molecule is embedded in the α-N_2 crystal very well and all of its excitations are strongly coupled to the host crystal lattice ones. The pure dephasing of the impurity vibrations is caused by anharmonic interactions with other modes of crystal. The librational motion of both the host crystal and the CO molecules becomes very anharmonic at temperatures higher than 30 K. Therefore, the higher order terms of the dephasing processes (eq 5) must be taken in account in this temperature region in principle.

The host crystal quality mainly affects the value of the coefficient B_{depop} in eq 5, whereas the B_{deph} and ω_{deph} values are just independent of crystal quality. This B_{depop} value increases noticeably in "bad" samples. This means that the depopulation relaxation processes are substantially more sensitive to the existence of crystal defects in comparison to the dephasing ones as expected.

(*b*) *Gaussian Component of the Bandwidth*. As in the case of the Lorentzian components, the temperature behavior of the Gaussian bandwidth components (Δ_G) is qualitatively similar for both substances. This similarity was more pronounced for high-quality samples. However, in the case of MI CO_2 in solid N_2, about 80% of the bandwidth possesses Lorentzian character, whereas, for CO the Lorentzian part equals the Gaussian one (Figures 3, 4).

As can be seen, the Gaussian component of the CO_2 bandwidth is almost constant at $T \leq 27$ K and increases slightly at higher temperatures. The plateau at low temperatures is less pronounced for the CO Gaussian bandwidth and extends to about 20 K only. The Gaussian bandwidths at low temperatures are about 0.01 cm^{-1} for MI CO_2 and CO; both values are close to the value (0.0068 cm^{-1}) of the Gaussian contribution to the vibron relaxation in the α-nitrogen obtained by time-resolved coherent anti-Stokes Raman scattering.[26] Dubost et al.[22] observed the pure Gaussian broadening in their CO spectra at the lowest CO concentration and $T \leq 20$ K ($\Delta = 0.02$ cm^{-1} at 20 K). The surprisingly strong contribution to Gaussian bandwidth broadening (as large as Lorentzian components) was observed for the CO internal vibrations at temperatures higher than 20 K.

According to common ideas,[25] a Gaussian broadening is caused by a static distribution of crystal defects and is temperature independent as long as this distribution is not changed: $\Delta_{inhomog}(T \rightarrow 0)$ mirrors therefore the crystal quality. If we rise temperature, especially close to a phase transition, many effects play an essential role which contribute to a temperature- or entropy-caused Gaussian broadening of the vibron bandwidth, which is not considered in the Lorentzian bandwidth: e.g., the time dependence of the instantaneous positions and mutual orientations of interacting particles, larger amplitudes, hopping processes, generation of vacancies. The instantaneous environmental frequency shift of the dissolved molecule is a function of the instantaneous positions and mutual orientations of interacting molecules. Therefore, the orientational and translational motions of both the guest and the host molecules lead to the corresponding distribution of the frequency values of a guest molecule. The first moment of this distribution expresses the environmental frequency shift observed by experiment $\Delta\omega = \omega_M - \omega_{gas}$, whereas the second moment corresponds to the Gaussian broadening of the guest molecule bandwidth. The explicit expression for the Δ_G in the self-consistent-field approximation (so-called "quasi-static broadening") is given in ref 3. Taking a librational motion of molecules into consideration only we obtain

$$(\Delta_G^2)_{quasistatic} \cong 8\ln(2)D^2[(1-\eta_g)^2\eta_{N_2}^2 + (1-\eta_{N_2})^2\eta_g^2 + (1-\eta_{N_2})^2(1-\eta_g)^2] \quad (6)$$

Here D is the effective force constant originating from the anisotropic part of the interaction between the guest and host molecules, and η_g and η_{N_2} are the orientational order parameters of the guest and host molecules, respectively. Because the CO_2 molecules are almost fixed in their equilibrium orientational positions ($\eta_{CO_2} \approx 1$), whereas the CO molecules join in the anharmonic librational motion together with the host crystal molecules ($\eta_{CO} \approx \eta_{N_2}$), eq 6 may be reduced as follows:

$$(\Delta_G^2)_{quasistatic}(CO_2) = 8\ln(2)D_{CO_2}^2(1-\eta_{N_2})^2 \quad (6a)$$

$$(\Delta_G^2)_{quasistatic}(CO) = 8\ln(2)D_{CO}^2(1-\eta_{N_2})^2(1-2\eta_{N_2}+3\eta_{N_2}^2) \quad (6b)$$

The total Gaussian bandwidth is given by the superposition of the inhomogeneous broadening originating from static crystal imperfections and the quasistatic broadening:

$$\Delta_G^2 = (\Delta_G^2)_{inhomog} + (\Delta_G^2)_{quasistatic}(T) \quad (7)$$

Using the eqs 6, 7, and the known experimental values of the N_2 orientational order parameter,[28] we fitted the experimental Gaussian components of the CO and CO_2 bandwidths. The results of this fitting procedure are shown by dotted lines in Figures 3 and 4. We obtained zero values of the inhomogeneous broadening for both substances, which means perfect crystals; the D values are as follows: 0.028 and 0.014 cm^{-1} for CO_2 and CO, respectively.

As can be seen, the quasistatic broadening mechanism explains the temperature dependence of the CO_2 Gaussian bandwidth but does not explain the strong temperature-caused Gaussian broadening of the CO bandwidth (Δ symbols in comparison to fit (dotted line)). This means we must take into account the direct dynamic coupling between the librations of the CO and N_2 molecules as well as the librational−translational coupling originating from the combined orientational motion of the CO molecule plus a deformed matrix area around it, which we neglected before in (6).

Using the results of our modeling of the Lorentzian and Gaussian components, we calculated the total full width at half-maximum for the $\nu_3(CO_2)$ band in α-nitrogen. The excellent agreement between the experimental and calculated values was achieved in the whole temperature region of the existence of α-N_2 (see Figure 3).

3.1.2. Mode Frequencies. The experimental values of the frequency of the fundamental modes of the ^{12}CO, ^{13}CO, $^{12}CO_2$, and $^{13}CO_2$ matrix isolated in the α-nitrogen as well as of the ^{12}CO overtone averaged over all our samples are presented in Table 3.

Our frequency values for the internal vibration of the CO isotopes coincide with the high-resolution data by others for

TABLE 3: Frequencies of the CO Fundamental and $\nu_3(CO_2)$ Vibration MI in Solid Nitrogen[a]

temp, K	$^{12}CO_2$	$13CO_2$	^{12}CO	^{13}CO	$\nu_{0-2}(^{12}CO)$
10.9	2349.09	2283.22	2139.78	2092.63	4253.05
14.8	2349.05	2283.18	2139.77	2092.61	4253.02
19.6	2348.95	2283.10	2139.73	2092.58	
24.6	2348.80	2282.96	2139.68	2092.54	
27.7	2348.69	2282.85	2139.64		
31.6	2348.52	2282.69	2139.58		
33.5	2348.42	2282.60	2139.54		
35.5	2348.31	2282.50	2139.49		

[a] All values are given in cm^{-1}; experimental inaccuracy ± 0.01 cm^{-1}.

similar concentrations of CO in the N_2 matrix at the same temperature range.[22] In the literature we found some values about the ν_3 vibration frequencies of the $^{12}CO_2$ and $^{13}CO_2$ MI in solid nitrogen, at temperatures 10 K,[20,29] 17 K,[21] and 20 K[18] and at much higher A/M ratios ($10^{-3}-10^{-2}$). The sets of data do not match each other.

Next, we want to show that the analysis of the temperature dependencies of the mode frequency of MI species can provide important information on the host crystal itself as well as on the mutual interaction between MI impurities and host crystal particles.

The "solvent shift" or matrix shift for the fundamental absorption bands in the pure matrix isolated case may be written in the following form, according to[2]

$$\Delta\omega_{0\to1}(\mathrm{CO}) = \frac{B_e}{\omega_e}\left\langle\left[\left(r^2\frac{\partial^2 U_{CO}}{\partial r^2}\right)_{r=r_e} + 3\sqrt{\frac{\omega_e x_e}{B_e}}\left(r\frac{\partial U_{CO}}{\partial r}\right)_{r=r_e}\right]\right\rangle \equiv \frac{B_e}{\omega_e}W_{CO} \quad (8a)$$

$$\Delta\omega_{0\to1}(\nu_3(CO_2)) = \frac{B_3}{\omega_3}\left\langle\left[r_e^2\left(\frac{\partial^2 U_{CO_2}}{\partial q^2}\right)_{q=0} - 6\frac{\omega_3 k_{331}}{\omega_1 B_3}\sqrt{\frac{B_1}{\omega_1}}\left(\rho\frac{\partial U_{CO_2}}{\partial \rho}\right)_{\rho=r_e}\right]\right\rangle \equiv \frac{B_3}{\omega_3}W_{CO_2} \quad (8b)$$

The equations (8) may be paraphrased in the following general formula to plot the scaled matrix shift for comparison:

$$W_g \equiv r_e^2\left\langle\left(\frac{\partial^2 U_g}{\partial q^2}\right)_{q=0}\right\rangle + K_g\left\langle\left(\rho\frac{\partial U_g}{\partial \rho}\right)_{\rho=r_e}\right\rangle = \left(\frac{B_q}{\omega_q}\right)^{-1}\Delta\omega_{0\to1} \quad (9)$$

Here, U_g is the intermolecular potential energy of the guest molecule; q is the normal coordinate of the guest molecule's internal vibration conjugated to the harmonic frequency ω_q and the measured frequency shift $\Delta\omega_{0\to1}$; ρ and r_e are the instantaneous and equilibrium bond length of the guest molecule, respectively (in the case of the CO_2 molecule r_e equals the distance between the oxygen atoms); B_q and K_g are the rotational constant and the coefficient composed of the guest molecule's spectroscopic constants corresponding to the analyzing frequency respectively, e.g.: $B_q = B_e$ and $K_g = 3\sqrt{\omega_e x_e/B_e}$ for diatomic molecules, $B_q = h/(8\pi^2\mu_3 c r_e)$ and $K_g = -6k_{331}(\omega_3/B_3)\sqrt{B_1/\omega_1^3}$ for an asymmetric vibration of a linear three-atomic molecule (x_e and k_{331} are the anharmonic constants of the free CO and CO_2 molecule, respectively; $\mu_3 = m_O m_C/(m_C + 2m_O)$, m_O and m_C are the mass of the oxygen and carbon atoms, respectively); the angular brackets denote the quantum mechanical and thermodynamic averaging over translational and orientational motion of both interacting particles.[2,3]

Because all molecular spectroscopic constants used in (9) are known with a high accuracy,[30−33] the function W_g provides direct experimental information on the forces acting between the guest molecule and the host crystal ones as well as on the changes in this interaction caused by the variation of internal conditions. The W_g values (eq 9) for the CO and CO_2 molecules matrix isolated in the α-nitrogen are shown as a function of temperature in Figure 5a,b.

The main factor that affects the frequency of MI species is the thermal expansion of the matrix as the temperature increases. The increase in the matrix volume by temperature changes the distance between the guest molecule and the surrounding host crystal particles directly and leads to the lowering of the orientational order parameter of both (host crystal and guest molecules) indirectly. Therefore, the function W_g may be expanded into the Taylor series with respect to the distance R between the guest molecule and the nearest neighboring host crystal particle at $R(0) \equiv R(T=0)$. We consider only the two first terms of this series, since the changes in R are relatively small at equilibrium vapor pressures:

$$W_g(T) \cong W_g(0) + \left(\frac{\partial W_g}{\partial R}\right)_{R=R(0)}[R(T) - R(0)] \quad (10)$$

The $W_g(0)$ values were obtained by extrapolating the experimental temperature dependencies shown in Figure 5a,b to zero temperature and are presented in the first column of Table 4 for all species investigated by us. Using these values of $W_g(0)$ together with the known experimental values of the nitrogen lattice parameter $R(T)$,[11] we can model the temperature dependencies of the W_g function with the formula (10) to determine the $(\partial W_g/\partial R)_{R=R(0)}$ values for each MI species separately (presented in Table 4). The results of this fitting procedure (lines in Figure 5a,b) coincide perfectly with the measured temperature dependencies of matrix shift of all four MI species.

Next, we would like to elaborate that the different matrix shifts $\Delta\omega_{0\to1}$ (Figure 5a,b) are actually very similar (Figure 5c) and have the same origin. The function W_g in (9) is composed of the first and second derivatives of the interaction energy U_g with respect to the corresponding normal coordinate of the solute at the equilibrium nuclear distances. These derivatives are described by similar functions of the coordinates of all (CO, CO_2, N_2) interaction particles and usually have the same order of magnitude. Therefore, the ratio of the terms in the function W_g (eq 9) is mainly determined by the coefficient K_g in front of the first derivative ($K_g = 7.8692$ for CO and $K_g = 62.7$ for CO_2). Then, for understanding the situation qualitatively, the first term in eq 9 may be neglected. This reduction leads to a small renormalization of the value of the first derivative of the intermolecular potential energy of the guest molecule relative to the true quantity only. In this approximation

$$W_g = K_g U' \approx K_g\left\langle\left(\rho\frac{\partial U_g}{\partial \rho}\right)_{\rho=r_e}\right\rangle \quad (9')$$

The variation of the U' values with temperature ($U'(T) - U'(0)$) for all of the MI species investigated by us is presented on Figure 5c. As can be seen, the temperature shift of the U' values is practically identical for all guest molecules; i.e., their temperature behavior is governed by the same physical mechanism. In other words, the measured mode frequency shift of MI molecules in a matrix as a function of T is ruled by the volume expansion of the matrix material. In reverse order, if one has measured the temperature dependence of matrix shift of an

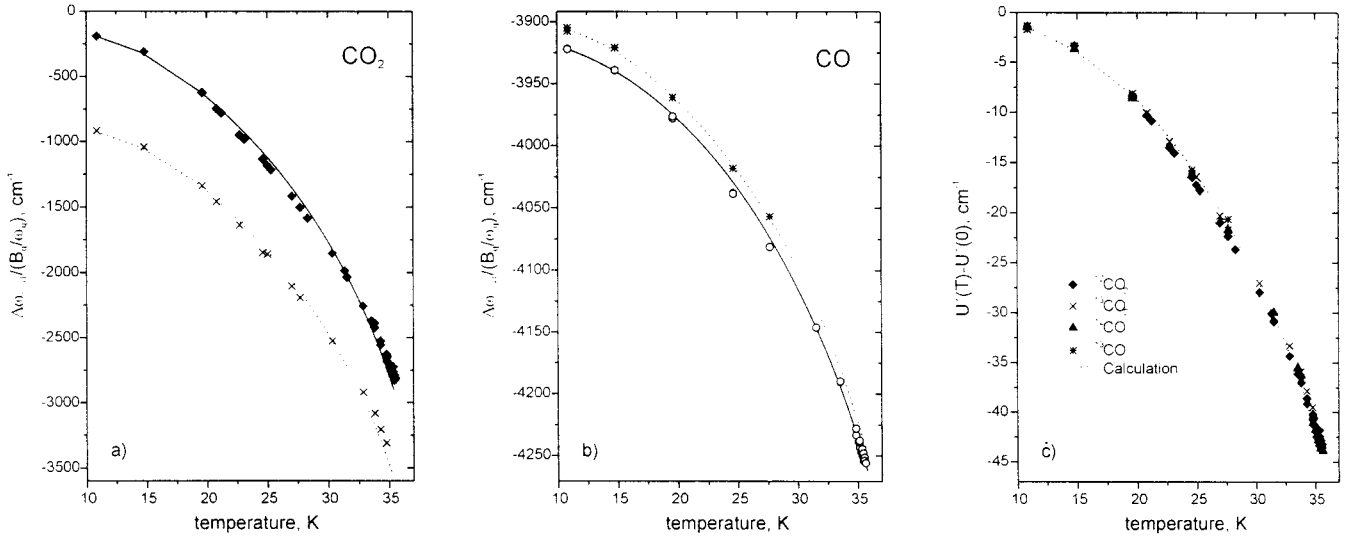

Figure 5. Normalized frequency shift of the internal vibrations of the MI molecules in α-nitrogen: (a) $^{12}CO_2$ (diamond, experiment; solid line, calculation); $^{13}CO_2$ (cross, experiment; dotted line, calculation); (b) ^{12}CO (circle, experiment; solid line, calculation); ^{13}CO (star, experiment; dotted line, calculation); (c) scaled normalized frequency shift using data points a and b.

TABLE 4: Normalized Matrix Shift for MI Species in α-Nitrogen[a]

substance	$W(R(0))$, cm^{-1}	$\partial W/\partial R\|_{R(0)}$, cm^{-1} Å^{-1}
$^{12}CO_2$	-101 ± 33	-80407 ± 467
$^{13}CO_2$	-829 ± 33	-79494 ± 864
^{12}CO	-3911 ± 11	-9942 ± 412
^{13}CO	-3894 ± 11	-9995 ± 305

[a]For details see eq 10.

impurity embedded in a matrix, whose volume expansion is not known, one can estimate this value.

Now we would like to discuss the isotope effect on the frequency shift of the guest molecule. As can be seen from Figure 5a,b and Table 4, the isotope shift of the W_g values has the opposite sign in the case of the CO and CO_2 molecules. The heavy CO isotope possesses the greater mass and the smaller rotational constant.[32,33] Therefore, these MI molecules are characterized by smaller amplitude of both translational and librational vibrations compared to the light isotope at the same parameters of a guest−host molecule interaction. Both of these effects result in smaller effective volume per guest molecule and consequently lead to the higher frequency of internal vibrations (Figure 5b). The isotope substitution of the carbon atom causes no changes in the molecular rotational quantum of the CO_2[31] and the increase of the molecular mass would have to cause a qualitatively similar isotope effect like in CO. We can only think of one reasonable explanation of the anomalous isotope effect for CO_2. The molecular parameters of $^{13}CO_2$ (quadrupole moment, polarizability, etc., or their derivatives with respect to the normal coordinate of the asymmetrical internal vibration) determining its interaction with the surrounding host particles are different from the parameters of the light CO_2 isotope, like in hydrogen.

3.2. Probing the Phase Transition in Solid Nitrogen. All spectroscopic characteristics of the guest molecules show some discontinuity at the α−β phase transition of solid N_2. The CO band became invisible in the β-N_2 and one CO_2 band in α-N_2 was split into two bands in the β-N_2 at exactly this transition (Figure 6). This fact was confirmed by simultaneous monitoring the behavior of the two-vibron band of N_2 that abruptly disappeared at α−β transition (Figure 6).

The two-vibron band temperature behavior in solid nitrogen will be discussed in more detail elsewhere.[34] There we will also explain why this band exists in the orientationally ordered α-phase of nitrogen only. In the present work, this IR-active host crystal band was used like an internal standard during our measurements to determine the point of the α−β phase transition in the solid nitrogen independently.

These changes in the spectroscopic characteristics of the guest molecules were completely reproducible by heating and cooling. Moreover, we clearly observed a thermal hysteresis of 0.2−0.3 K for the α−β phase transition in solid N_2 by monitoring the behavior of impurity bands (showed areas in Figure 7a,b). This hysteresis was best distinct in the case of CO_2 spectra (Figure 7a,b) because both the frequency and the bandwidth of the ν_3-(CO_2) internal vibrations show a clear jump at the α−β phase transition in solid N_2. Furthermore, we observed the coexistence region of the α- and β-phases and were able to watch the growth of crystal of the β-phase of solid nitrogen recording the spectra of MI species as a function of time at a fixed temperature (Figure 7c).

This means that by monitoring the MI molecule carefully we can not only observe the phase transition in the host crystal and clarify the order of this transition but also investigate the kinetics of this transition and the hysteresis phenomena.

The existence of two bands for the $\nu_3(CO_2)$ fundamental mode in β-N_2 is a strong indicator for the fact that two possible orientations of molecules exist in the hcp structure of β-N_2. The total intensity of two CO_2 bands in the β-nitrogen is equal to the intensity of the CO_2 peak in the α-N_2 at the transition point within experimental error. The high-temperature β-phase of solid nitrogen is characterized by a rotational disorder at zero pressure. Because the CO_2 molecules possess a moment of inertia 5 times larger than the N_2 molecules, they cannot join in a thermal orientational motion of matrix molecules but are almost fixed in equilibrium orientational positions. In these positions the CO_2 molecules can accomplish a librational motion only. In contrast to the CO_2 molecules, the CO impurity molecule is almost identical to the matrix molecule and takes part in the orientational motion together with them. Because of the strong rotational−translational coupling as well as the multiplicity of possible orientational positions, the CO fundamental becomes very wide in β-N_2 and therefore cannot be observed at such small concentrations of the CO molecules ($\sim 10^{-7}$).

3.3. $\nu_3(CO_2)$ Bands in β-Nitrogen. As the temperature

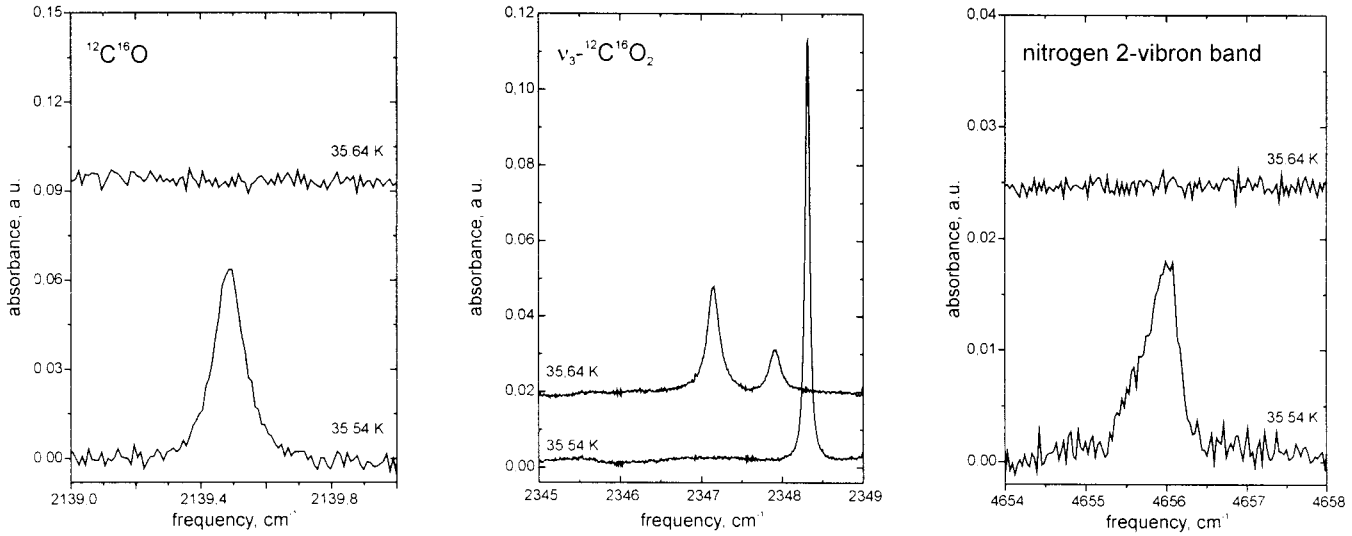

Figure 6. IR spectra in vicinity of the $\alpha \rightarrow \beta$ phase transition in solid nitrogen at $T = 35.54$ K and at 35.64 K.

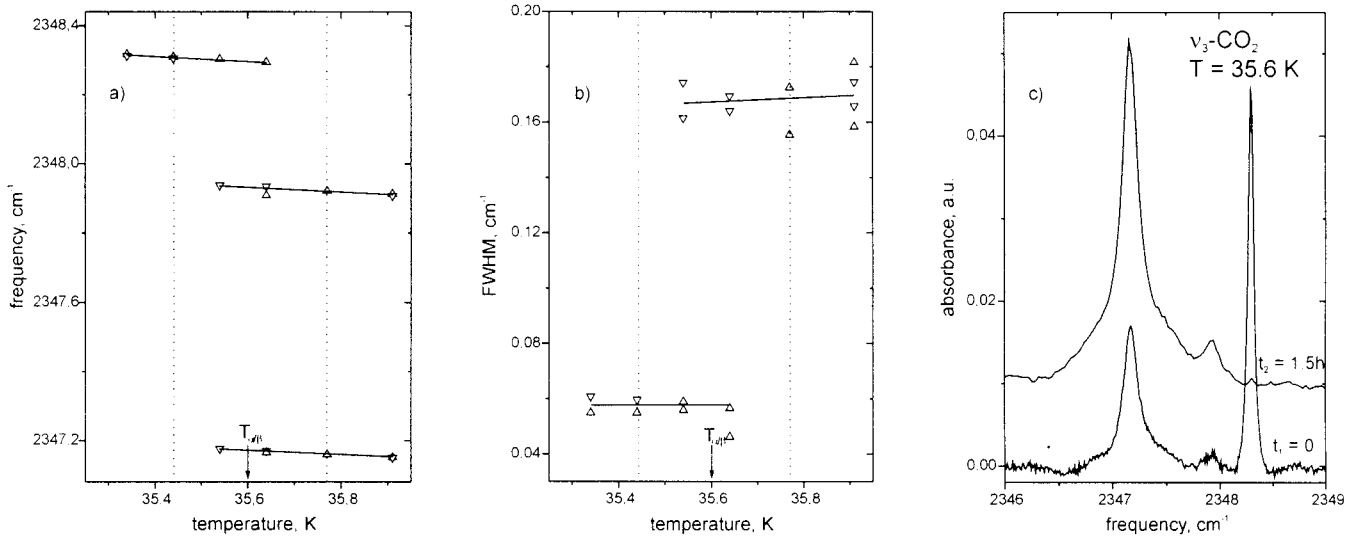

Figure 7. Thermal hysteresis of the $\alpha \rightarrow \beta$ phase transition in solid nitrogen observed by monitoring ν_3 excitations of CO_2 molecules MI in solid nitrogen ($CO_2/N_2 \sim 1.3 \times 10^{-7}$): (a) frequency (triangle up, heating; triangle down, cooling); (b) bandwidth (triangle up, heating; triangle down, cooling); vertical lines around the phase transition $T_{\alpha\beta}$ indicate the temperature interval for this hysteresis; (c) spectra recorded at 35.6 K just after a temperature increase and 1.5 h later: the band due to CO_2 in α-N_2 is decreased, which means that regions of β-N_2 in the sample are growing.

increases the frequencies of the $\nu_3(CO_2)$ bands (Figure 8a) are shifted to lower values due to the thermal expansion of the N_2 matrix. We used eq 10 to describe the frequency temperature dependency. Because the deviation of the hexagonal structure from an ideal hcp structure is very small at zero pressure in β-N_2, the R values used in the calculations (eq 10) were averaged corresponding to the formula $R = 1.3292(V_{mol})^{1/3}$, where V_{mol} is the molar volume for the β-nitrogen.[11] The excellent agreement between experimental values and the fit function (eq 10) was achieved for both vibrational bands of CO_2 with the following parameters:

$$W_1(35.64\ \text{K}) = -6600 \pm 15\ \text{cm}^{-1},\ (\partial W_1/\partial R)_{R=R(35.64\ \text{K})} = -81579 \pm 760\ \text{cm}^{-1}\ \text{Å}^{-1}$$

$$W_2(35.64\ \text{K}) = -4030 \pm 15\ \text{cm}^{-1},\ (\partial W_2/\partial R)_{R=R(35.64\ \text{K})} = -96093 \pm 864\ \text{cm}^{-1}\ \text{Å}^{-1}$$

for the low-frequency (index 1) and high-frequency (index 2) bands, respectively.

The values of the $\partial W_g/\partial R$ for both CO_2 bands in the β-N_2 were close to the corresponding value for CO_2 in α-nitrogen (see Table 4). This is strong evidence for the fact that the CO_2 molecules remain strictly localized in certain orientational positions in the β-N_2 too, like in α-N_2. For example, in the case of the N_2 vibron excitations the values of the W_g derivatives for the α- and β-phases are different by a factor of more than 4. Obviously, this is because the α-phase is characterized by an existence and the β-phase by an absence of the long-range orientational order.

The temperature-caused broadening of both CO_2 bands in the β-N_2 is just the same below 42 K and becomes qualitatively different at higher temperatures (Figure 8b). Whereas the low-frequency band maintains almost the same increase in broadening in the whole temperature region (35.6−50 K), the high-frequency one starts to increase very quickly at temperatures higher than 42 K. We observe a pure Lorentzian line shape for both bands within the inaccuracy of the peak fit procedure near the $\alpha-\beta$ phase transition and up to 42 K. At higher temperatures the contribution of a Gaussian broadening to this high-frequency peak bandwidth becomes nonnegligible and reaches about 60%

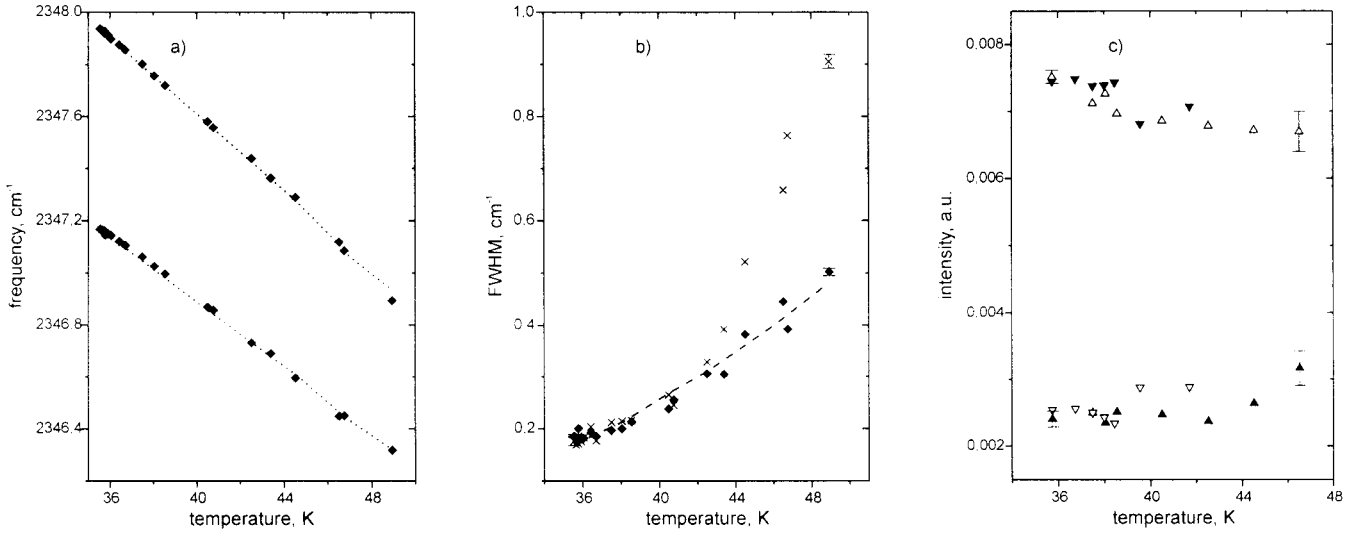

Figure 8. Spectroscopic qualities of the $\nu_3(CO_2)$ vibration in β-nitrogen: (a) frequency (diamond, experiment; dotted line, calculation); (b) bandwidth (diamond, low-frequency peak; cross, high-frequency peak; dashed line, calculation); (c) intensity: low-frequency peak (solid triangle up, heating; open triangle down, cooling), high-frequency peak (open triangle up, heating; solid triangle down, cooling). In general, error bars are smaller than symbols, unless indicated.

of this bandwidth at 50 K (Figure 8b). It is interesting to note that for the N_2 vibrons in the β-nitrogen a qualitatively similar but quantitatively smaller increase of the Gaussian contribution to the internal vibration bandwidth was observed in ref 23.

The profile analysis of the two CO_2 bands shows that the fit parameters for a Lorentzian band shape of both CO_2 bands almost coincide and can be described by the same function of the temperature. Using eq 5, we find $B_{\mathrm{depop}} = 0$, $B_{\mathrm{deph}} = 5.32 \pm 1\ \mathrm{cm}^{-1}$, and $\omega_{\mathrm{deph}} = 87.5 \pm 5.2\ \mathrm{cm}^{-1}$ (dotted line in Figure 8b). The frequency of the localized mode (ω_{deph}) to determine the CO_2 bandwidth Lorentzian broadening by dephasing processes is just the same in both solid nitrogen phases. It is the second indication of the librational character of the CO_2 orientational motion in β-nitrogen.

The total intensity of two $\nu_3(CO_2)$ bands is independent of the temperature within the inaccuracy of the peak fit procedure, whereas the intensity ratio of the low- and high-frequency bands tends to decrease as the temperature increased: from about 3.1 near the $\alpha-\beta$ transition to 2.1 at 50 K (Figure 8c). These intensity changes are accompanied by a decrease of the energy splitting between the $\nu_3(CO_2)$ bands from 0.77 cm^{-1} at 35.6 K to 0.57 cm^{-1} at 50 K. These changes in the spectroscopic characteristics of the CO_2 internal vibration bands are completely reproducible by cooling and heating.

We assigned these two bands in our spectra of MI CO_2 in β-N_2 to two possible orientations of CO_2 in β-N_2. To explain the origin for these two kinds of orientational positions of MI CO_2 in the β-nitrogen we want to understand the situation in general at first. Because β-nitrogen possesses no long-range orientational order, we ignore the orientational degrees of freedom of the matrix in our model analysis. This means that only the isotropic part of the guest−host intermolecular interaction is taken into account.

For the interaction potential V_{gm} (g = guest, m = matrix) between the triatomic linear guest molecule and mth host crystal particle, we used the force site interaction potential in the following form:

$$V_{\mathrm{gm}}(R_{\mathrm{m}},\theta,\varphi) = \sum_i 4\epsilon_{iM}\left\{\left(\frac{\sigma_{iM}}{r_{im}}\right)^{12} - \left(\frac{\sigma_{iM}}{r_{im}}\right)^{6}\right\} \qquad (11)$$

where R_{m} is the distance between the centers of mass of the guest molecule and the matrix particle on the mth position in the host crystal; θ and φ are the Euler angles of the guest molecule's axis relative to the hexagonal axis of the host crystal structure ($\theta = 0-\pi$, $\varphi = 0-2\pi$); r_{im} is the distance between ith atom of a guest molecule ($i = 1, 2, 3$) and the center of mass of mth matrix molecule; ϵ_{iM} and σ_{iM} are the mixed Lennard-Jones potential parameters describing the interaction between the ith atom of the guest molecule and the host crystal molecule (M indicates host crystal particles in general). These parameters can be obtained by usual combination rules,[14] e.g. $\epsilon_{iM} = \sqrt{\epsilon_{ii}\epsilon_{MM}}$ and $\sigma_{iM} = (\sigma_{ii} + \sigma_{MM})/2$. The distances R_{m} and r_{im} may be described by the following formula:

$$R_{\mathrm{m}} = R_0 k_m;$$
$$r_{im} = R_0[(k_m)^2 + (\xi_i)^2 - 2\xi_i k_m(\vec{\omega}\vec{n}_m)]^{1/2} \equiv R_0 f_{im} \quad (12)$$

Here, R_0 is the radius of the first coordination sphere of a host crystal; $\vec{\omega}$ is the unit vector along the molecule axis, and $\vec{n}_m = \vec{R}_m/R_m$; $\xi_i = d_i/R_0$, d_i is the distance from the center of mass to the ith atom within the guest molecule (d_i may have both positive and negative signs corresponding to the ith atom position relative to the vector $\vec{\omega}$). The k_m value corresponds to the relative distance between the centers of mass of the guest molecule and mth matrix particle and is completely determined by the host crystal structure, whereas the f_{im} value in addition depends on the ξ_i parameter as well as on the orientation of the guest molecule in a matrix.

On substituting (12) into (11) and summing over the whole host crystal ($\sum_m$), we obtain the general formula for the guest molecule potential energy

$$V_{\mathrm{g}} = 4\sum_i e_{iM}\left(\frac{\sigma_{iM}}{R_0}\right)^6\left[\left(\frac{\sigma_{iM}}{R_0}\right)^6\sum_m f_{im}{}^{-12} - \sum_m f_{im}{}^{-6}\right] \qquad (13)$$

In the case of the symmetric triatomic MI molecule, the guest molecule's center of mass coincides with the central atom c and eq 13 reads as follows:

$$V_g = 4\epsilon_{cM}\left(\frac{\sigma_{cM}}{R_0}\right)^6\left[\left(\frac{\sigma_{cM}}{R_0}\right)^6\sum_m {k_m}^{-12} - \sum_m {k_m}^{-6}\right] + 4\epsilon_{oM}\left(\frac{\sigma_{oM}}{R_0}\right)^6\sum_m\left[\left(\frac{\sigma_{oM}}{R_0}\right)^6({f_{(+d)_m}}^{-12} + {f_{(-d)_m}}^{-12}) - ({f_{(+d)_m}}^{-6} + {f_{(-d)_m}}^{-6})\right] \quad (13')$$

The ϵ_{cM}, σ_{cM} and ϵ_{oM}, σ_{oM} indicate the interaction parameters of the matrix particle *M* with the central and outside atoms of a guest molecule, respectively. The indices (+d) and (−d) mark the outside atoms located in the positive and negative directions relative to the vector $\vec{w}$.

Because only the second term in (13′) depends on the guest molecule orientation, we will paraphrase this formula in a dimensionless form suited to our analysis:

$$U(R,\omega) = \sum_m\left[\left(\frac{\sigma_{oM}}{R_0}\right)^6(f_{(+d)m}^{-12} + f_{(-d)m}^{-12}) - (f_{(+d)m}^{-6} + f_{(-d)m}^{-6})\right] = \left\{V_g - 4\epsilon_{cM}\left(\frac{\sigma_{cM}}{R_0}\right)^6\left[\left(\frac{\sigma_{cM}}{R_0}\right)^6\sum_m k_m^{-12} - \sum_m k_m^{-6}\right]\right\}/\left[4\epsilon_{oM}\left(\frac{\sigma_{oM}}{R_0}\right)^6\right] \quad (14)$$

The function *U* determines the orientational potential relief for the guest molecule in a host crystal matrix and depends on the ξ value ($\xi = d/R_0 \equiv r_e/(2R_0)$) as well as on details of the host crystal structure.

The quantitative analysis of this potential relief was carried out by the symbolic computer algebra program Maple V Release 5. The interaction of the guest molecule with 80 neighboring N_2 molecules located in the eight coordination spheres of the hcp structure was taken into account. To calculate $(\sigma_{oM}/R_0)^6$ the Lennard-Jones parameters of the oxygen atom and N_2 molecule as well as the averaged R_0 value of the β-N_2[11] were used; i.e., $\sigma_{OO} = 2.88$ Å,[5] $\sigma_{N_2N_2} = 3.708$ Å,[8] and $R_0 = 4.078$ Å. The results of our analysis are shown in Figure 9. It is very important to note that the numerical values of the coefficient $(\sigma_{oM}/R_0)^6$ in (14) ($(\sigma_{oM}/R_0)^6 = 0.276$ in our case) influence the numerical values of *U* but do not affect the qualitative conclusions drawn below.

Let us analyze the potential relief for the symmetric linear molecule trapped in the ideal hcp matrix ($c/a = \sqrt{8/3}$) as a function of the bond length/intermolecular distance ratio r_e/R_0 (Figure 9, left side).

In the case of small r_e/R_0 values ($r_e/R_0 = 0.2$) the only kind of orientational positions exists in hcp structure (Figure 9, left below). The potential energy minimum corresponds to the angle $\vartheta_{min} \approx \pi/3$ relative to the normal to the closed-packed layers of the hexagonal host crystal structure and is 6-fold degenerate: $\varphi_{min} = (\pi/6)k$ ($k = 0, 1, ...$). Because these minima are very shallow ($U_{max} - U_{min} = 0.02$), a guest molecule can be localized in these positions at very low temperatures only. As the r_e/R_0 value increases the potential relief becomes more pronounced, the existing potential minima are weakly shifted toward $\theta = \pi/2$, and the new minimum in the guest molecule's potential energy appears at $\theta = 0$ (the case of $r_e/R_0 = 0.4$ in Figure 9). At the following increase of r_e/R_0 values the depth of both potential wells ($\theta \approx \pi/3$ and $\theta = 0$) becomes comparable ($r_e/R_0 = 0.57$, Figure 9 above).

The last $r_e/R_0 = 0.57$ value is equal to the bond length/intermolecular distance ratio in the case of the CO_2 molecules trapped in the β-nitrogen: $(r_e)_{CO_2} = 2.3242$ Å,[31] $R_0 = 4.078$ Å. The potential barriers, corresponding to the case $r_e/R_0 = 0.57$, are high enough to localize the MI CO_2 molecules in both orientational positions in the N_2 matrix (Figure 9 top, positions 1 and 2). Indeed, substituting, e.g., the intermolecular interaction parameters ϵ_{OO}, $\epsilon_{N_2N_2}$ given[5,8] into (13′), we obtain the potential barrier height values larger than 200 cm^{-1}.

Thus, we have an explanation for the two orientations of the CO_2 molecules on substitutional sites in β-N_2 that give rise to two bands in the IR spectra. On the contrary, CO molecules, whose bond length/intermolecular distance ratio corresponds to $r_e/R_0 = 0.27$, possess only one minimum of the potential energy in β-N_2, generating one band in the absorption spectra. Recently, similar results were obtained for some linear molecules trapped in solid parahydrogen at helium temperatures.[35] The authors observed two kinds of bands for the CO_2 and N_2O molecules and only one for the CO at the same conditions.

Next, we would like to make some considerations about the intensity ratio of these two CO_2 components (Figure 8c) on the basis of this model. The lower potential energy minimum at $\theta \approx \pi/3$ is favored with respect to the higher minimum at $\theta = 0$ and the occupation ratio for these two minima is proportional to the Boltzmann factor multiplied by the ratio of the degeneracy orders of these orientational positions (6 and 1 for the $\theta_{min} \approx \pi/3$ and $\theta_{min} = 0$ respectively):

$$\frac{n(\theta\approx(\pi/3))}{n(\theta=0)} \sim 6\exp\left[-\frac{V_g(\theta\approx(\pi/3)) - V_g(\theta=0)}{kT}\right] > 1 \quad (15)$$

Therefore, we obtain the following assignment of two CO_2 bands in the β-nitrogen: the low-frequency band corresponds to the orientational position at $\theta_{min} \approx \pi/3$ (position 1 in Figure 9 top) whereas the high-frequency one to the orientational position at $\theta_{min} = 0$ (position 2 in Figure 9, top).

The second factor, which may influence the shape of the potential relief for the guest molecule, is the difference between the real host crystal structure and an ideal hcp lattice characterized by the difference in the *c*/*a* ratios. Since the deviations of the *c*/*a* parameter in the pure β-nitrogen from an ideal hcp structure are very small (1.631−1.636[11] compared to $(c/a)_{ideal} = \sqrt{8/3} \approx 1.633$) they cannot affect the above-mentioned results significantly. However, there is an additional effect due to a local deformation of the matrix around the guest molecules localized in two orientational positions. The deformation field in a matrix reproduces the guest molecule's shape. Therefore, the *c*/*a* ratios in the deformed matrix area around the impurity are qualitatively different for two the kinds of orientational positions: the $(c/a)_{def} - (c/a)_{id.hcp}$ value is positive for the orientational position at $\theta = 0$ and negative in the case $\theta \approx \pi/3$. Because the matrix's deformations are mainly localized in the first coordination sphere and decrease very fast for next shells,[7] we may model the local matrix deformation in our calculations by introducing the deviation from the ideal *c*/*a* value for the first coordination sphere into (14). The results of such modeling are shown in Figure 9 too (right side). The negative deviation from the ideal *c*/*a* value ($c/a = \sqrt{8/3} - 0.02$) pronounces the potential minima and maxima, whereas the positive deviation ($c/a = \sqrt{8/3} + 0.02$) flattens the potential barriers. This kind of consideration shows that the shape of the potential relief for the guest molecule is very sensitive to the

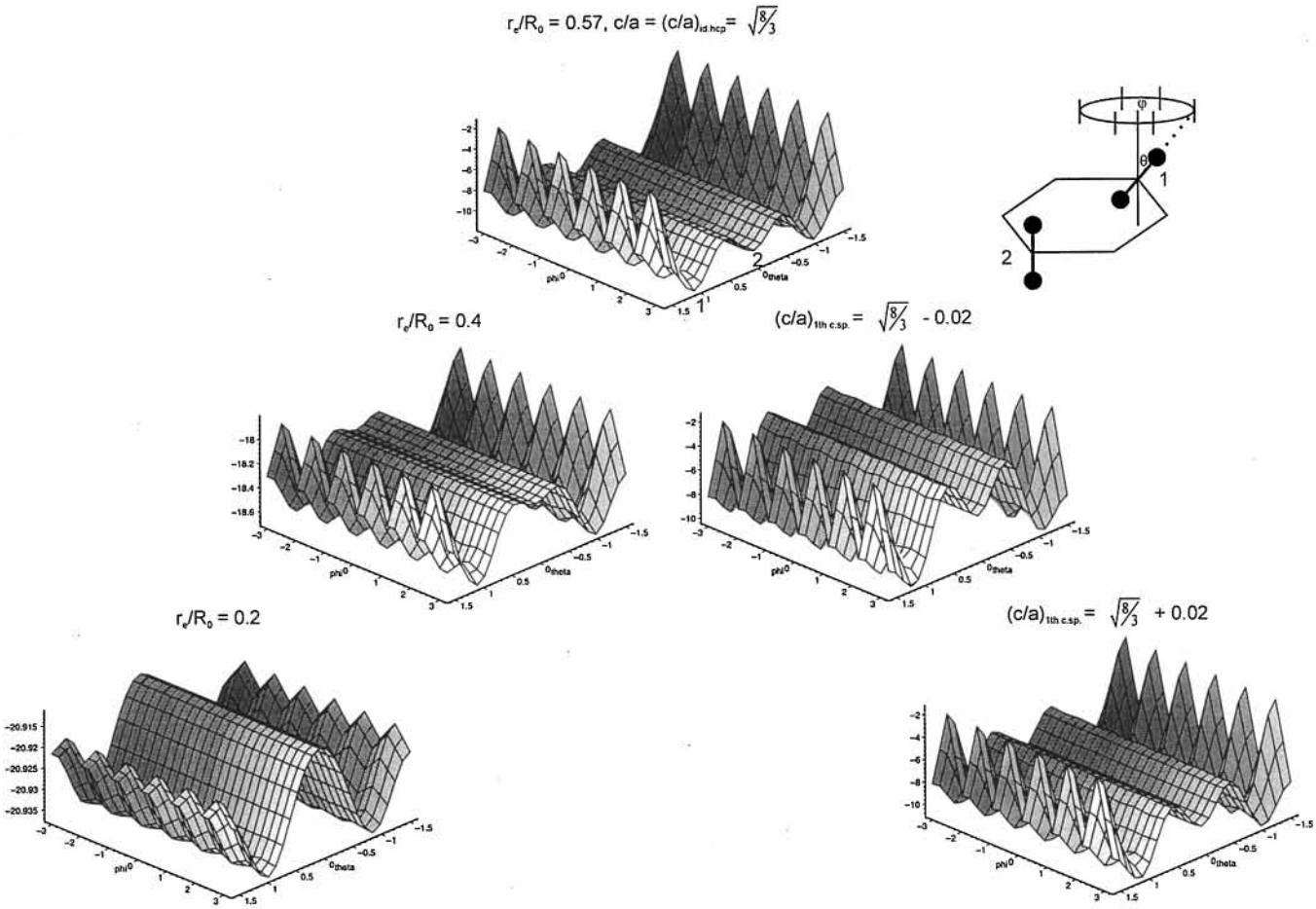

Figure 9. Potential energy of the guest molecule as a function of the ratio between bond length and intermolecular distance (left part) as well as the hcp lattice distortion (right part).

local deformation of a matrix around the impurity and, consequently, the deformation effects must be reflected in the behavior of the spectroscopic characteristics of the guest molecules, e.g., in the intensity ratio of the two bands in hcp structure.

This model can now be exploited to explain the unusual broadening of one of the $\nu_3(CO_2)$ components in β-N_2. Because of the shallower potential well at $\vartheta = 0$ the librational motion of the CO_2 molecules occupying these orientational positions is characterized by a larger amplitude in comparison to the molecules localized at $\theta_{min} \approx \pi/3$. The larger amplitude in the position $\theta = 0$ for CO_2 in β-N_2 causes stronger fluctuations of the local crystal field due to either the anharmonicity of the librational motion or due to the rotational−translational coupling of the molecule in the deformed matrix cage. Consequently, the high-frequency band, assigned to the CO_2 position at $\theta = 0$, must possess a stronger Gaussian broadening at higher temperatures, as it does (Figure 8b).

3.4. CO_2 Clusters in the Solid Nitrogen. In the samples with 75 ppm of CO_2 we observe a broad feature (width ∼50 cm^{-1}) in the range of the ν_3 fundamental mode of $^{12}C^{16}O_2$ (Figure 10a). The sharp peak corresponding to the ν_3 excitations of the CO_2 molecules matrix isolated in solid nitrogen is located at the top of this broad band. Whereas this sharp peak clearly reacted on the temperature changes as well as on the $\alpha-\beta$ transition in solid nitrogen, the broad band remains insensitive to any changes in the nitrogen matrix behavior up to 90 K. At such high temperatures (∼90 K) only some changes in the shape of this broad band are observed. The shape of this band, at temperatures corresponding to a gaseous N_2, is very similar to the $\nu_3(CO_2)$ band profile observed by Ewing and Sheng[36] for CO_2 ultrafine particles in Ar gas at a CO_2/Ar dilution equal to 1/600. According to the estimation of the authors,[36] these ultrafine CO_2 particles consisted out of about 200 CO_2 molecules. Therefore, we associated this band in Figure 10a with small CO_2 clusters in nitrogen. The spectral changes in the band shape of CO_2 cluster in the liquid and gaseous nitrogen in comparison to solid nitrogen may be caused by cluster coagulation at high temperatures.

This assignment above is also confirmed by the observation of the additional absorption (bandwidth ∼2−4 cm^{-1}) for $^{13}C^{16}O_2$ isotopes at about 2282.8 cm^{-1} (10.9 K). This band remains practically invariant in the whole temperature region from 11 to 90 K (Figure 10b), whereas the sharp peak for the $^{13}CO_2$ molecules trapped in the α-N_2 showed clear dependence on the temperature (Figure 10b, peak with *). Therefore, we assigned the relatively broad band (2−4 cm^{-1}) to an absorption by the $^{13}CO_2$ molecules trapped in the clusters of about 200 $^{12}CO_2$ molecules.

The position and bandwidth of this $^{13}CO_2$ isotope band are consistent with spectra of $^{13}CO_2$ as natural contamination in bulk CO_2 crystal[29,37,38] as well as in CO_2 clusters.[39−41] Since the frequency of this isotope band CO_2 is lying at 2280.6 cm^{-1} in amorphous CO_2[29] and at 2282.6 cm^{-1} in crystalline CO_2,[29] we may conclude that our CO_2 clusters possess crystalline quality.

The detailed analysis of the isotope $^{13}CO_2$ band profile shows that this band in fact consists of two bands marked by "M" and "D" in Figure 10b. The intensity ratio I_D/I_M of these two bands ranges between 6.4×10^{-2} and 7.5×10^{-2} and shows no

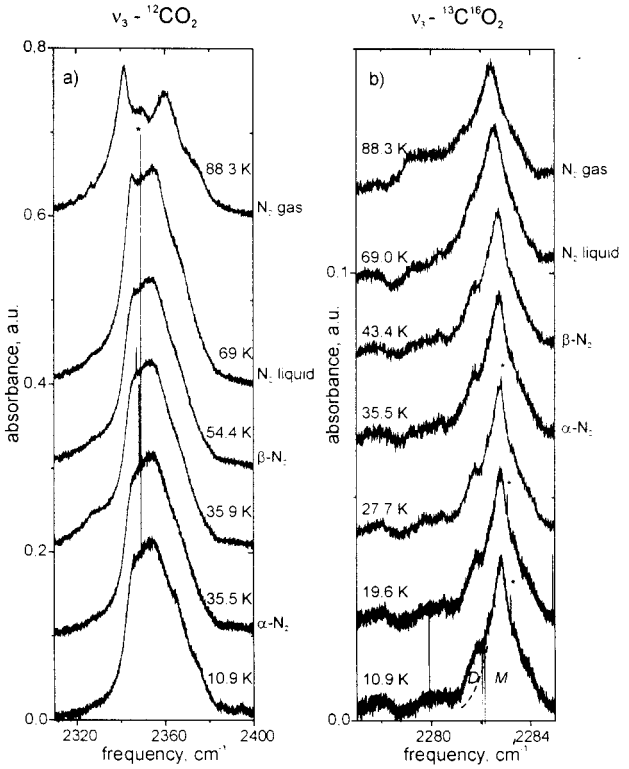

Figure 10. Spectra in the $\nu_3(CO_2)$ region of CO_2 clusters in nitrogen (75 ppm of CO_2 in N_2) at different temperatures: (a) for $^{12}CO_2$ clusters, peak * due to matrix-isolated $^{12}CO_2$ in N_2; (b) for $^{13}CO_2$ molecules in $^{12}CO_2$ clusters (M, monomer; D, dimer), peak * due to matrix-isolated $^{13}CO_2$ in N_2.

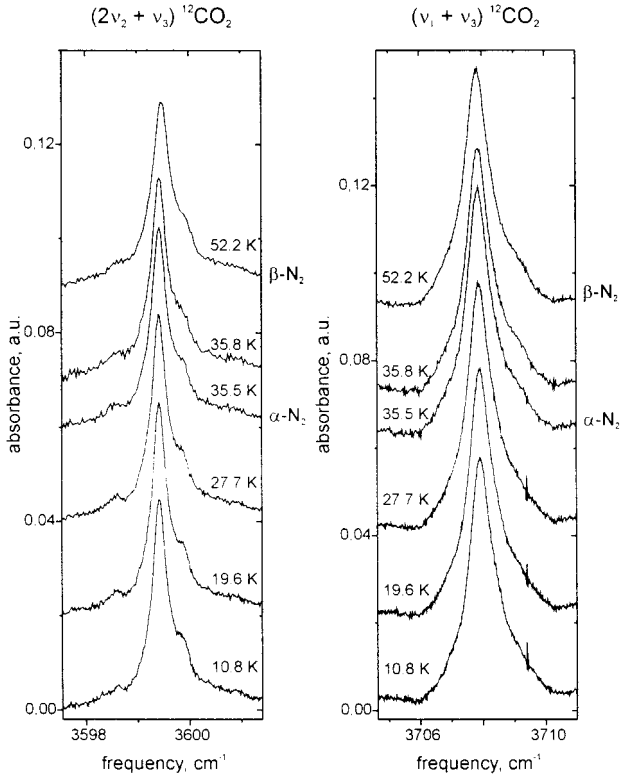

Figure 11. Combination bands of CO_2 clusters in nitrogen (75 ppm of CO_2 in N_2) at several temperatures.

marked dependence on temperature. This value for the intensity ratio I_D/I_M is close to a numerical value (0.11) describing the ratio of pair to single impurities of 1% impurities in an fcc lattice with stochastic distribution.[44] Therefore, we suggest the following assignment (Figure 10b): peaks M and D correspond to the $^{13}C^{16}O_2$ monomer (one $^{13}C^{16}O_2$ molecule is surrounded by 12 $^{12}CO_2$ molecules) and to the $^{13}C^{16}O_2$ dimer (one $^{13}C^{16}O_2$ molecule is surrounded by 11 $^{12}CO_2$ and 1 $^{13}C^{16}O_2$ molecules) in $^{12}CO_2$ clusters, respectively. Since the theoretical value (0.11) and our experimental value (0.06−0.07) differ quite substantially, we may think about two possible explanations: either the calculations[44] are not completely valid for mesoscopic systems or the absorption coefficients of a monomer and a dimer of the $^{13}CO_2$ in a $^{12}CO_2$ matrix are slightly different.

The last important observation was that the combined $^{12}CO_2$ bands ($2\nu_2 + \nu_3$ and $\nu_1 + \nu_3$) appeared as relative sharp features in our spectra (Figure 11). These CO_2 bands are also insensitive to the $\alpha-\beta$ transition in solid nitrogen. The centers of gravity of these bands correspond to 3599.6 and 3708.1 cm^{-1} at 10.9 K for the $2\nu_2 + \nu_3$ and $\nu_1 + \nu_3$ CO_2 excitations, respectively. The $2\nu_2 + \nu_3$ band shows practically no temperature dependence in the temperature region from 11 to 52 K, whereas the $\nu_1 + \nu_3$ is slightly shifted toward lower frequencies as the temperature increased (approximately 0.1 cm^{-1}/40 K). The frequency values of both bands agree very well with spectra of crystalline CO_2.[38−40]

The sharp character of the isotope $^{13}CO_2$ (Figure 10b) band and the $^{12}CO_2$ combined bands (Figure 11) as well as the good agreement in frequencies of these absorption spectra with the ones of crystalline CO_2 provide convincing proof that the CO_2 clusters observed by us in the nitrogen doped with 75 ppm of CO_2 had a crystalline structure like in bulk CO_2. This statement agrees with the result of investigations by electron diffraction of CO_2 clusters formed in a free jet expansion[42] that even CO_2 clusters consisting of 90 molecules possess cubic bulk structure. The comparison of the $\nu_3(^{12}CO_2)$ band shape in our spectra with the spectroscopic results in refs 40 and 43 and the theoretical calculations in ref 43 shows that the small crystalline CO_2 clusters were well separated from each other in our nitrogen matrix.

The existence of the CO_2 crystalline clusters in the samples doped with 75 ppm of CO_2 allows us to now explain why the intensities of the MI CO_2 bands were just the same in both series of our samples (low and high concentration of CO_2); both type of samples were slowly grown from the liquid phase at equilibrium conditions. We interpret this specific result as a strong evidence for the fact that CO_2 molecules do not practically dissolve in condensed nitrogen phases. The thermodynamic equilibrium solubility limit for the CO_2 in solid nitrogen lies at about (or less) 1 ppm of CO_2 in N_2 due to our results.

4. Conclusion

We have used the matrix-isolated technique to render fundamental information on the host crystal as well as on the MI species. We carefully investigated the *real* matrix-isolated cases (the impurity/matrix ratio was less than 10^{-6}) for CO_2 and CO molecules in solid nitrogen at the equilibrium vapor pressure by high-resolution Fourier transform infrared spectroscopy between 10 and 100 K. Our absorption spectra, as a function of temperature and two concentrations of CO_2 in N_2, in the mid-IR region were assigned to vibrations and their overtones of CO and CO_2 and their isotopes. Our analysis of these spectra exploited the bandwidth, band maximum, and band shape as a function of temperature and concentration.

On the basis of the precise analysis of the bandwidth of MI species we discovered for the first time the temperature-caused Gaussian contribution to the MI species bandwidth broadening. The modeling of the experimental temperature dependence of

the broadening of the Lorentzian bandwidth for both MI species showed that the low energetic N_2 librational excitations are mainly responsible for the vibronic dephasing of CO molecules dissolved in the α-nitrogen, whereas broadening of the Lorentzian bandwidth of MI CO_2 by dephasing processes is governed by localized modes which are caused by perturbations of the N_2 crystal lattice by these guest molecules. We put emphasis on the strong influence of the rotational−translational coupling on the bandwidth of MI species caused by the intense librational motion of the guest molecules in the matrix.

Some important parameters of the intermolecular interaction between guest molecules and matrix were reconstructed from a careful analysis of the temperature dependence of the frequencies of these guest molecules.

The anomalous isotope effect was observed for the CO_2 molecules in the α-nitrogen in comparison to CO and a possible explanation is proposed. Two qualitatively different kinds of the orientational positions of the guest molecules were discovered in β-nitrogen and a theoretical model of this phenomenon is presented. The qualitative conclusions of this model are valid for any hcp structure.

Finally, starting from the real matrix-isolated case, we can determine the thermodynamic equilibrium solubility limit by changing the concentration of the impurity molecules; this limit is about 1 ppm of CO_2 in solid N_2. In the samples with 75 ppm of CO_2 in N_2 we observed crystalline clusters of about 200 CO_2 molecules, which were well separated in the nitrogen matrix. We even observed the $^{13}CO_2$ dimers within these $^{12}CO_2$ clusters.

We have shown, by monitoring the impurity molecule in the *real* matrix-isolated case that we can (1) observe the phase transitions in the host crystal, clarify the order of these transitions, and determine exactly the transition point as well as investigate the hysteresis phenomena; (2) find out possible orientational positions of the MI molecule in the host crystal; and (3) estimate indirectly changes in the host crystal volume when these data are unknown.

References and Notes

(1) *Vibrational spectroscopy of trapped species*; Hallam, H. E., Ed.; John Wiley & Sons: New York, 1973.

(2) Buckingham, A. D. *Faraday Soc. Trans.* **1960**, *56*, 26.

(3) Brodyanski, A. P.; Jodl, H. J. "Vibron−libron coupling in cryocrystals: theory and applications", to be published.

(4) Guasti, R.; Schettino, V.; Brigot, N. *Chem. Phys.* **1978**, *34*, 391. Irvine, M. J.; Mathieson, J. G.; Pullin, A. D. E. *Aust. J. Chem.* **1982**, *35*, 1971. Winn, J. S.; *J. Chem. Phys.* **1991**, *94*, 5275.

(5) Dahoo, P. R.; Berrodier, I.; Raducu, V.; Teffo, J. L.; Chabbi, H.; Lakhlifi, A.; Abouaf-Marguin, L. *Eur. Phys. J. D* **1999**, *5*, 71.

(6) Stoneham, A. M. *Theory of defects in solid;* Clarendon Press: Oxford, UK, 1975.

(7) Brodyanskii, A. P.; Strzhemechny, M. A. *Sov. J. Low Temp. Phys.* **1990**, *16*, 203

(8) Manzhelii, V. G.; Prokhvatilov, A. I.; Minchina, I. Ya.; Yantsevich, L. D. *Handbook of Binary Solutions of Cryocrystals;* Begel House: New York, 1996.

(9) *Gas encyclopaedia*; Engl. transl. by Nissim Marshall; Elsevier: Amsterdam, 1976.

(10) *Tables of Isotopes*, 7th ed.; Lederer, C. M., Shirley, V. S., Eds.; Wiley: New York, 1978.

(11) *Physics of cryocrystals*; Manzhelii, V. G., Freiman, Yu. A., Eds.; AIP: Woodbury, NY, 1997.

(12) Varasani, P.; Sarangi, S. *J. Quant. Spectrosc. Radiat. Transfer* **1975**, *15*, 473. Schurin, B.; Ellis, R. E. *J. Chem. Phys.* **1966,** *45*, 2528. Korb, C. L.; Hunt, R. H.; Plyler, E. K. *J. Chem. Phys.* **1968,** *48*, 4252

(13) Legay, F.; Legay-Sommaire, N. *Chem. Phys.* **1982**, *65*, 49.

(14) Mason, E. A.; Spurling, T. H. In *The international Encyclopedia of Physical Chemistry and Chemical Physics*; Rowlinson, J. S., Ed.; 1968; Vol. 2.

(15) Bader, R. F. W.; Bandrauk, A. D. *J. Chem. Phys.* **1968**, *49*, 1653.

(16) Kihara, T.; Sakai, K. *Acta Crystallogr. Sect. A* **1978**, *34*, 326.

(17) Di Bartolo, B.; *Optical Interactions in Solids*; John Wiley & Sons: New York, 1968.

(18) Fredin, L.; Nelander, B.; Ribbegard, G. *J. Mol. Spectrosc.* **1974**, *53*, 410.

(19) Carr, B. R.; Chadwick, B. M.; Edwards, C. S.; Long, D. A.; Wharton, F. C. *J. Mol. Struct.* **1980,** *62*, 291

(20) Dilella, D. P.; Tevault, D. E. *Chem. Phys. Lett.*, **1986**, *126*, 38.

(21) Nxumalo, L. M.; Ford, T. A. *J. Mol. Struct.* **1994**, *327*, 145.

(22) Dubost, H.; Charneau, R.; Harig, M. *Chem. Phys.* **1982**, *69*, 389.

(23) Ouillon, R.; Turc, C.; J-Lemaistre, P.; Ranson, P. *J. Chem. Phys.* **1990**, *93*, 3005

(24) Beck, R. D.; Hineman, M. F.; Nibler, J. W. *J. Chem. Phys.* **1990**, *92*, 7068.

(25) Foggi, P.; Schettino, V. *Rivi. Nuovo Cimento* **1992**, *15*, 1.

(26) De Kinder, J.; Goovaerts, E.; Bouwen, A.; Schoemaker, D. *Phys. Rev.* **1990,** *42*, 5953

(27) Diestler, D. J.; Zewail, A. H. *J. Chem. Phys.* **1979**, *71*, 3103; *J. Chem. Phys.* **1979**, *71*, 3113. Robert, D.; Galatry, L. *J. Chem. Phys.* **1976**, *64*, 2721

(28) Scott, T. A. *Phys. Rep.* **1976**, *27C*, 89.

(29) Falk, M. *J. Chem. Phys.* **1987**, *86*, 560.

(30) Suzuki, I. *J. Mol. Spectrosc.* **1968**, *25*, 479.

(31) Guelachvili, G. *J. Mol. Spectrosc.* **1980**, *79*, 72.

(32) Mantz, A. W.; Maillard, J-P.; Roh, W. B.; Narahari Rao, K. *J. Mol. Spectrosc.* **1975**, *57*, 155.

(33) Chen, D-W.; Narahari Rao, K. *J. Mol. Spectrosc.* **1976**, *61*, 71.

(34) Vetter, M.; Brodyanski, A. P.; Jodl, H. J. "Origin of IR-active two-vibron bands in molecular crystal: investigation of two-vibron bands in α-nitrogen and γ-oxygen by high-resolution FTIR spectroscopy", to be published.

(35) Fajardo, M. Private communication, 1999.

(36) Ewing, G. E.; De Sheng, T. *J. Phys. Chem.* **1988**, *92*, 4063.

(37) Cahill, J. E. *J. Chem. Phys.* **1977**, *66*, 4847.

(38) Dows, D. A.; Schettino, V. *J. Chem. Phys.* **1973**, *58*, 5009.

(39) Barnes, J. A.; Gough, T. E. *J. Chem. Phys.* **1987**, *86*, 6012.

(40) Ovchinnikov, M. A.; Wight, C. A. *J. Chem. Phys.* **1993**, *99*, 3374.

(41) Fleyfel, F.; Devlin, J. P. *J. Phys. Chem.* **1989**, *93*, 7292.

(42) Torchet, G.; Bouchier, H.; Farges, J.; de Feraudy, M. F.; Raoult, B. *J. Chem. Phys.* **1984**, *81*, 2137.

(43) Ovchinnikov, M. A.; Wight, C. A. *J. Chem. Phys.* **1994**, *100*, 972.

(44) Behringer, R. E. *J. Chem. Phys.* **1958**, *29*, 537.